In Situ Observation of Calcium Aluminate Inclusions Dissolution into Steelmaking Slag

KEYAN MIAO, ALYSSA HAAS, MUKESH SHARMA, WANGZHONG MU, and NESLIHAN DOGAN

The dissolution rate of calcium aluminate inclusions in CaO-SiO_2-Al_2O_3 slags has been studied using confocal scanning laser microscopy (CSLM) at elevated temperatures: 1773 K, 1823 K, and 1873 K (1500 °C, 1550 °C, and 1600 °C). The inclusion particles used in this experimental work were produced in our laboratory and their production technique is explained in detail. Even though the particles had irregular shapes, there was no rotation observed. Further, the total dissolution time decreased with increasing temperature and decreasing SiO_2 content in the slag. The rate limiting steps are discussed in terms of shrinking core models and diffusion into a stagnant fluid model. It is shown that the rate limiting step for dissolution is mass transfer in the slag at 1823 K and 1873 K (1550 °C and 1600 °C). Further investigations are required to determine the dissolution mechanism at 1773 K (1500 °C). The calculated diffusion coefficients were inversely proportional to the slag viscosity and the obtained values for the systems studied ranged between 5.64×10^{-12} and 5.8×10^{-10} m^2/s.

https://doi.org/10.1007/s11663-018-1303-y
© The Minerals, Metals & Materials Society and ASM International 2018

I. INTRODUCTION

INCLUSION formation during liquid steel refining is an unavoidable consequence of current steel making processes. The nature and quantity of the inclusions formed in steel is critical, as it affects both productivity and in-service properties of steel. These inclusions can be controlled by two approaches; the modification of their composition and morphology, or the removal of inclusions to the waste slag phase.

Oxide and sulfide inclusions can be modified with the addition of calcium using powder injection or wire feeding. A well-known example is the modification of solid alumina inclusions into liquid, or partially liquid, calcium aluminate inclusions. There has been a debate about the correct reaction between dissolved calcium [Ca] and Al_2O_3 inclusions. Traditionally, the reactions of Al_2O_3 inclusions in calcium treatment were proposed as Eqs. [1] and [2] to form various types of calcium aluminate inclusions[1–3]

$$x[\mathrm{Ca}] + \left(1 - \frac{2}{3}x\right)\mathrm{Al_2O_3} = x\mathrm{CaO} \cdot (1-x)\mathrm{Al_2O_3} + \frac{2}{3}x[\mathrm{Al}], \quad [1]$$

$$x\mathrm{CaO} + y\mathrm{Al_2O_3} = x\mathrm{CaO} \cdot y\mathrm{Al_2O_3}. \quad [2]$$

The melting point of calcium aluminates increases with increasing alumina concentration, to form stable solid inclusions at steelmaking temperatures. Insufficient or superfluous addition of calcium leads to incomplete or excessive modification of alumina inclusions and the formation of unwanted inclusions such as $CaO{\cdot}2Al_2O_3$ and $CaO{\cdot}6Al_2O_3$ that can cause clogging of submerged entry nozzles at continuous casting.

The resulting inclusions would ideally be removed from the liquid steel to slag in the ladle, tundish, or caster mold prior to solidification. Therefore, it is important to understand the inclusion–slag interaction towards improving the removal of inclusions from liquid steel. During ladle refining, inclusions are transported to the steel–slag interface where they are separated from steel and dissolved in the slag. Fast dissolution kinetics helps to prevent the re-entrainment of inclusions into liquid steel. Inclusions are similarly removed by tundish/mold flux during casting, where rapid dissolution also prevents early crystallization within the slag that may lead to sticker breakouts.[4,5] Research on inclusion removal in steel refining falls into three main categories: (i) flotation of inclusions to the steel/slag

KEYAN MIAO, ALYSSA HAAS, MUKESH SHARMA, and NESLIHAN DOGAN are with the Steel Research Centre, Department of Materials Science and Engineering, McMaster University, 1280 Main Street West, Hamilton, ON L8S 4L7, Canada. Contact e-mail: miaok@mcmaster.ca WANGZHONG MU is with the Department of Materials Science and Engineering, Royal Institute of Technology in Stockholm, Brinellvägen 8, Stockholm, 100 44, Sweden.

Manuscript submitted August 10, 2017.
Article published online June 4, 2018.

interface,[6,7] (ii) physical separation of inclusions into the slag phase,[8,9] and (iii) dissolution of inclusions in the slag phase.[4,5,10–18]

Early research data[17,19–21] that are relevant to the kinetics of inclusion removal have been obtained by using a technique in which a cm-size refractory rod is immersed in a slag for a period of time, removed, and then analyzed for slag corrosion and/or penetration. Although much has been learned using this approach, the difference in scale from bulk materials to small inclusions is likely to have a significant bearing on the dissolution kinetics of inclusions in a slag, and this difference will also influence capillary effects. Additionally, data from an indirect (dip test) procedure rely on a comparison of the initial and final conditions of a sample. Therefore, the changes in sample size and morphology during the dissolution process were not discussed in detail, and some of the key kinetics parameters such as diffusion coefficients were not reported. The dynamic wetting characteristics of slag on any inclusion are a critical factor strongly affecting the inclusion's bonding or reactivity with slag. Maximizing removal efficiency implies maximizing attachment strength. The inclusion should be highly wettable by slag, and have a fast dissolution rate in the slag.

The confocal scanning laser microscopy (CSLM) technique overcomes the drawbacks of the dipping technique. CSLM allows for continuous *in situ* observation of micron-size samples in real time. This is a unique feature of this technique that would not be possible by most other conventional imaging techniques in the conditions that are relevant to the steelmaking process. CSLM was first used for steel research by Emi *et al.*[22–24] to study crystal growth during solidification in Fe-C melts. Since then it has been used to examine dynamic changes such as particle collision, cluster formation, and solidification.[25–30]

Several researchers[4,5,10–12,15,31] have applied the CSLM technique to study the dissolution behavior of a single oxide particle in slag. High-resolution, fast scanning rates of the microscope and quantitative analysis of the images provide vital information about the kinetics and mechanisms of inclusion dissolution. Using CSLM, Monaghan and Chen,[15,31] Liu *et al.*,[10] and Valdez *et al.*[5,11,12] confirmed that dissolution of alumina particles is mass transfer controlled in the slag phase and that these results are consistent with those from the dipping technique. However, it is not clear whether the mass transfer coefficients and diffusion coefficients generated by these two different techniques are consistent. This question still needs to be addressed. Further, the CSLM technique has so far been applied to limited inclusion types, such as Al_2O_3, $MgAl_2O_4$, MgO, and SiO_2. There are no data available for calcium aluminate inclusions, Ti-containing inclusions, and sulfide inclusions that are of interest to a number of steelmakers. Given the industrial importance of inclusion removal in steelmaking, this area requires fundamental study to fill the gaps in our knowledge.

Calcium dialuminate ($CaO{\cdot}2Al_2O_3$) inclusions are harmful to productivity and steel properties.[32] With limited time between calcium injection and tapping, the formation of solid calcium aluminates is inevitable. The work presented here investigated the effect of temperature and slag composition on the dissolution rate of $CaO{\cdot}2Al_2O_3$ (CA_2) particles using CSLM. As a rather novel research tool in comparison to some other dissolution research approaches, the limitation of the CSLM technique is also discussed.

II. EXPERIMENTAL APPROACH

A. *Materials*

Many of the stoichiometric or non-stoichiometric compounds comprising the inclusion types formed during steelmaking processes are not commercially available from reagent suppliers. This limits the assessment and testing of key inclusion groups important in steelmaking so these inclusion materials have to be made under reproducible conditions in order to provide firm base for experimentation. For this purpose, the authors adapted reported techniques for making high-purity calcium dialuminate particles (CA_2).[33]

As starting materials, $CaCO_3$ and Al_2O_3 powders purchased from Sigma Aldrich. A 200 g charge of 33 wt pct $CaCO_3$ and 67 wt pct Al_2O_3 powders was mixed in a ball mill for an hour to homogenize. A slurry was then made by pouring this oxide powder mixture into 500 mL deionized water. The slurry was vacuum filtered in a Buchner funnel through Whatman #6 filter papers with a pore diameter of 3 μm. Particles retained on the filter papers were dried in an oven at 353 K (80 °C) for 24 hours. The dried powder was moistened with approximately 4 wt pct distilled water after removal from the filter papers, and 7 to 10 g of mixed powder was then pressed into 2.5 cm diameter × 1 cm thick pellets at a load of 200 MPa.

The pellets (all at once) were placed in an alumina crucible and sintered in a muffle furnace at an initial heating rate of 10 K per minute from room temperature to 1173 K (900 °C), held at this temperature for one hour, and then heated to the sintering temperature of 1673 K (1400 °C) and held for 24 hours followed by furnace cooling to room temperature. The sintered pellets were then hand crushed into powders and analyzed using X-ray diffraction (XRD). The XRD pattern of crushed powder is shown in Figure 1. No other phases were identified *via* XRD. This finding indicates successful production of high-purity substance. The CA_2 powder was re-pelletized and sintered using the similar procedures described. The second sintering was performed at 1873 K (1600 °C), which is 200 K higher than the first sintering process to reduce the porosity of the particles, which were used in dissolution experiments.

Particle densities measured using a pycnometer at room temperature were found to be 2761 ± 89 kg/m^3 compared with reported values of 3000 and 3150 kg/m^3.[34,35] The difference between measured and reported

values for CA_2 density might be due to differences between measurement techniques as well as the porosity of the particles in this study. A comparison between measured and reported values suggests that our sintered CA_2 particles have 10 to 14 vol pct porosity. The particle density was corrected for expansion at experimental temperatures using Eq. [3].[36] The linear thermal expansion coefficient of CA_2 is available for temperatures up to 1173 K (900 °C).[34] The expansion coefficient was extrapolated to 1550 °C assuming a linear increase with temperature from 973 K to 1823 K (700 °C to 1550 °C), a reasonable assumption because it is reported that the densities of CaO and Al_2O_3 expand linearly with temperature from 727 K to 2227 K (1000 °C to 2500 °C).[37] The extrapolated mean CA_2 linear thermal expansion coefficient α_L, equals 5.2×10^{-6}/°C.

$$\rho = \frac{\rho_0}{1 + 3\alpha_L \Delta T}, \qquad [3]$$

where ρ_0 and α_L denote density at room temperature and linear thermal expansion coefficient, respectively, and ΔT denotes the temperature difference. Assuming isotropic behavior and applying the linear thermal expansion coefficient,[34] CA_2 density was calculated and equals approximately 2694 kg/m^3 at 1823 K, with a range less than 2 kg/m^3 between 2692 and 2696 kg/m^3. For simplicity, it is assumed that particle density remains constant from 1773 K to 1873 K (1500 °C to 1600 °C).

Two synthetic slags composed of 30.5 CaO, 23.2 Al_2O_3, 46.3 SiO_2, and, 56.1 CaO, 38.6 Al_2O_3, 5.2 SiO_2, all in weight percent, were used for CSLM experiments. The high SiO_2 content slag is referred as slag 1 (S1) and the low SiO_2 slag is slag 2 (S2). Slags studied in this work contained no transition elements so both slags are transparent to the CSLM imaging system. To prepare the slag, high-purity oxide powders of appropriate proportions were initially mixed and then heated to a temperature, 50 K higher than the slag liquidus temperature, to completely melt in a 0.4 mL platinum crucible. After homogenization of molten slag at this temperature for 30 minutes, slags were quenched and crushed. This process was repeated twice to ensure slag homogeneity. The compositions of resultant slags were confirmed by the inductively coupled plasma optical emission spectrometry (ICP-OES) analysis. The slags were then hand crushed to very fine powder, in order to minimize the number of gas bubbles trapped. Approximately 0.1 g of crushed slag powder was compacted in a platinum crucible (10 mm OD × 5 mm height) and remelted in a vertical tube furnace at the same temperature above its liquidus to be used in the dissolution experiments, and held under vacuum for 30 seconds to reduce the gas bubbles entrapped in molten slag.

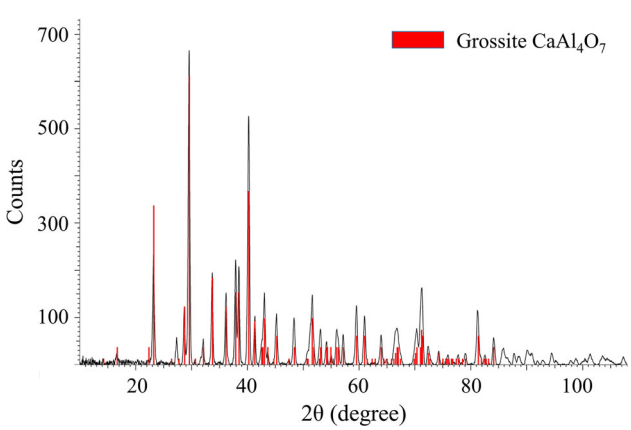

Fig. 1—XRD pattern of CA_2 particles sintered at 1673 K (1400 °C) (Color figure online).

B. *Experimental Procedure*

A Lasertec VL2000DX-SVF17SP confocal laser scanning microscope was used in this study. Below the furnace chamber, there is a halogen (1.5 kW) lamp used as a heating element and a light source. A 405 nm laser light source further improves the image resolution and features with a diameter of 0.5 μm can be resolved. A programmable temperature controller supports rapid heating and cooling rates up to 1000 K/min (°C/min) with a maximum temperature of 1973 K (1700 °C). Rapid quenching at 1000 K/min can be achieved by flowing He gas through the crucible chamber.

The experimental setup is schematically illustrated in Figure 2. Technical details of the CSLM have been published elsewhere.[22] The temperature was measured using B type thermocouple, attached to the bottom of the crucible holder. A single CA_2 particle was placed on the surface of the pre-molten slag in a platinum crucible. The particle, sample holder, and crucible were heated to the experimental temperature under high-purity (99.999 pct) Ar atmosphere. Before entering the chamber, Ar passes through a gas purification system to remove the dust in the gas system. Once slag was liquid, the particle was completely covered by slag before experimental temperatures were reached. We define time zero as the moment when the experimental temperature was reached. The experiments were repeated three times at each temperature to confirm reproducibility.

Figure 3 provides the thermal cycle of dissolution experiments. The sample was heated to 1273 K (1000 °C) at a rate of 100 K/min, then the temperature was elevated to experimental temperature using a heating rate of 150 K/min. It was held at the experimental temperature during the dissolution process and cooled to room temperature with a cooling rate of 100 K/min. Sample surface temperature was correlated to the thermocouple temperature by observing melting of iron (purity > 99.9 pct, melting point 1811 K (1538 °C)), which showed that the surface temperature of the sample is 63 ± 5K (°C) higher than that of thermocouple temperature. This temperature difference was considered to apply throughout this work.

All of the experiments were captured by a charge couple device (CCD) camera that was positioned above the sample. Hence, only particle projection on the horizontal plane was captured. The oxide particle was distinguished from the slag based on the contrast in each frame. In some cases, the contrast between the particle

and slag was insignificant. The brightness and contrast of images were adjusted to obtain a distinct clear boundary.

Figure 4 shows a series of images of a dissolving CA_2 particle in slag 1 (S1) at 1823 K (1550 °C). The particle can be found in the center of each image and the white lines represent the slag–particle interface. It is clear that the particle projection on the horizontal plane decreases over time. It can be seen that the actual shape of the sintered particles is far from spherical, and it is very difficult to express the volume evolution of irregular particles using a single parameter that changes over time. In this work, the dissolving particles were assumed to be spherical for simplicity. The areas bounded by white lines were then measured using image processing program, ImageJ. The equivalent radii of a particle were calculated based on their projection on the horizontal plane. It is important to note that CA_2 particles rarely rotated and moved slowly in the slag. They were always

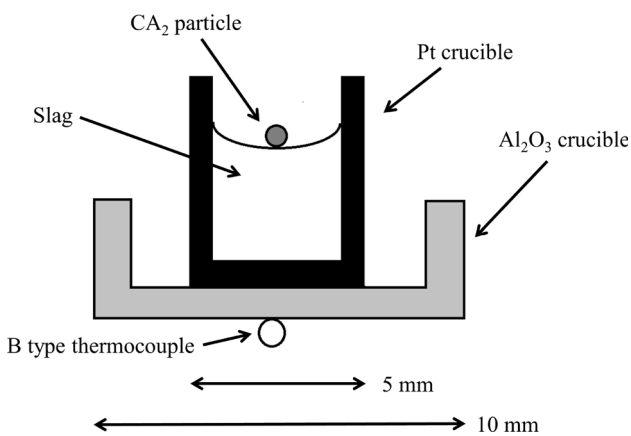

Fig. 2—Schematic diagram of sample and crucible configuration in CSLM.

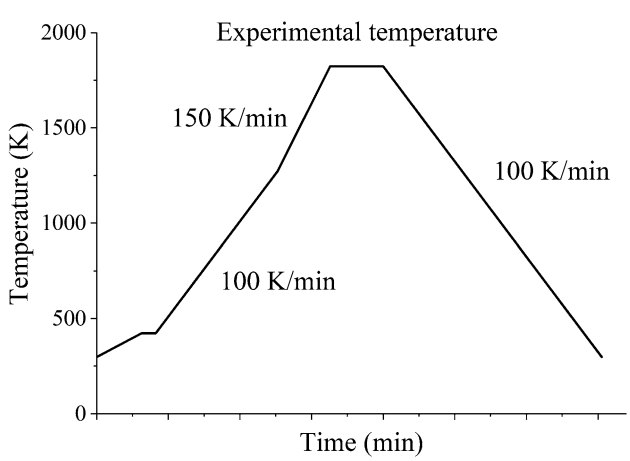

Fig. 3—Schematic diagram of the thermal cycle used for inclusion dissolution experiments.

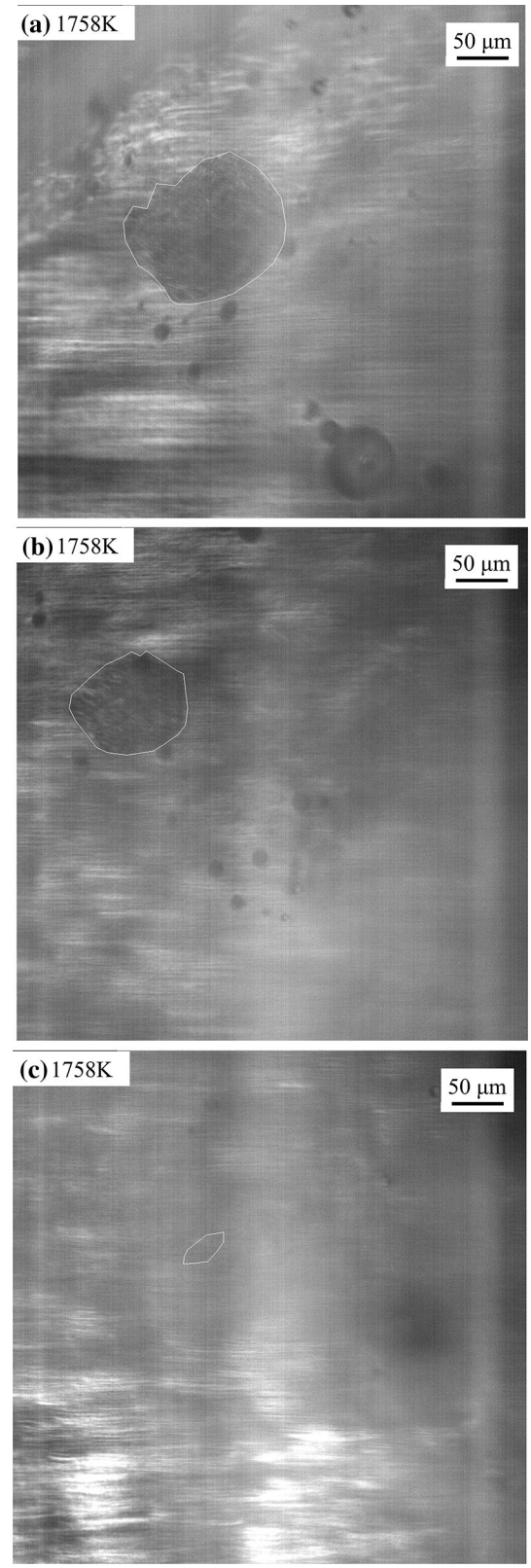

Fig. 4—Images of dissolution process of a single CA_2 particle in slag 1 at 1823 K (1550 °C) at (*a*) 24.54 s (*b*) 67.95 s (*c*) 120.16 s.

suspended in the CaO-SiO_2-Al_2O_3 slags during dissolution process at the temperature range from 1773 K to 1873 K (1500 °C to 1600 °C). Hence, it is assumed that the particle dissolved uniformly in all directions.

III. RESULTS AND DISCUSSION

A. *Thermodynamic Analysis*

To understand the effects of both temperature and slag composition on the dissolution rate of CA_2 particles better, the stable phases that may be present in the CaO-SiO_2-Al_2O_3 slag-CA_2 particle system at 1773 K, 1823 K, and 1873 K (1500 °C, 1550 °C, and 1600 °C) were calculated using FactSage™ as shown in Figures 5(a) through (c), respectively. The initial composition of slag 1 and slag 2 is marked in Figure 5. Both types of slag are in the fully liquid region at the temperature range that is studied. The dashed lines are the two-phase tie lines and the dotted lines represent the expected changes in slag composition. It should be noted that experiments with slag 2 at 1773 K (1500 °C) were not conducted because slag 2 was not fully liquid at that temperature.

The reaction paths shown in Figure 5 indicate that the formation of new phases is possible. For slag 1, CA_6 is expected as an intermediate product over the entire temperature range studied. In order to confirm the formation of reaction product, a slag–particle sample was quenched using He gas at 60 seconds after reaching experimental temperature, with the particle fully submerged. The quenched slag and CA_2 particle were ground to expose a cross section of particle–slag system. Figure 6 shows the scanning electron microscopy (SEM) back scattered images at 140 times magnification for a single CA_2 particle–slag 1 interface. The dark gray area at the center represents the CA_2 particle, whereas light gray area represents the slag 1. The black spots are pores inside the sintered particle. The two white lines labeled as Line Data 1 and Line Data 2 locate the two energy dispersive spectroscopy (EDS) line scans conducted on the surface. The results of the EDS line scans are shown in Figure 7.

In Line Data 1, the distance between 250 and 650 μm corresponds to the cross section of the CA_2 particle. The data from 0 to 250, and 650 to 950 μm represent the slag. In Line Data 2, the CA_2 particle is located between 170 and 610 μm, the rest of the EDS data represents the slag. The sudden drop in counts corresponds to the pores on the EDS scanning path in Figure 6. There are clear concentration gradients of Al (green) and Si (blue) detected in both Line Data 1 and 2. The concentration gradients indicate the boundary layer formed between the slag bulk and the slag–particle interface. No reaction products such as CA_6 were detected in this work. This may be because the formation of reaction product is unlikely to nucleate during a dissolution process, or, it might be very thin and difficult to detect by line scan.

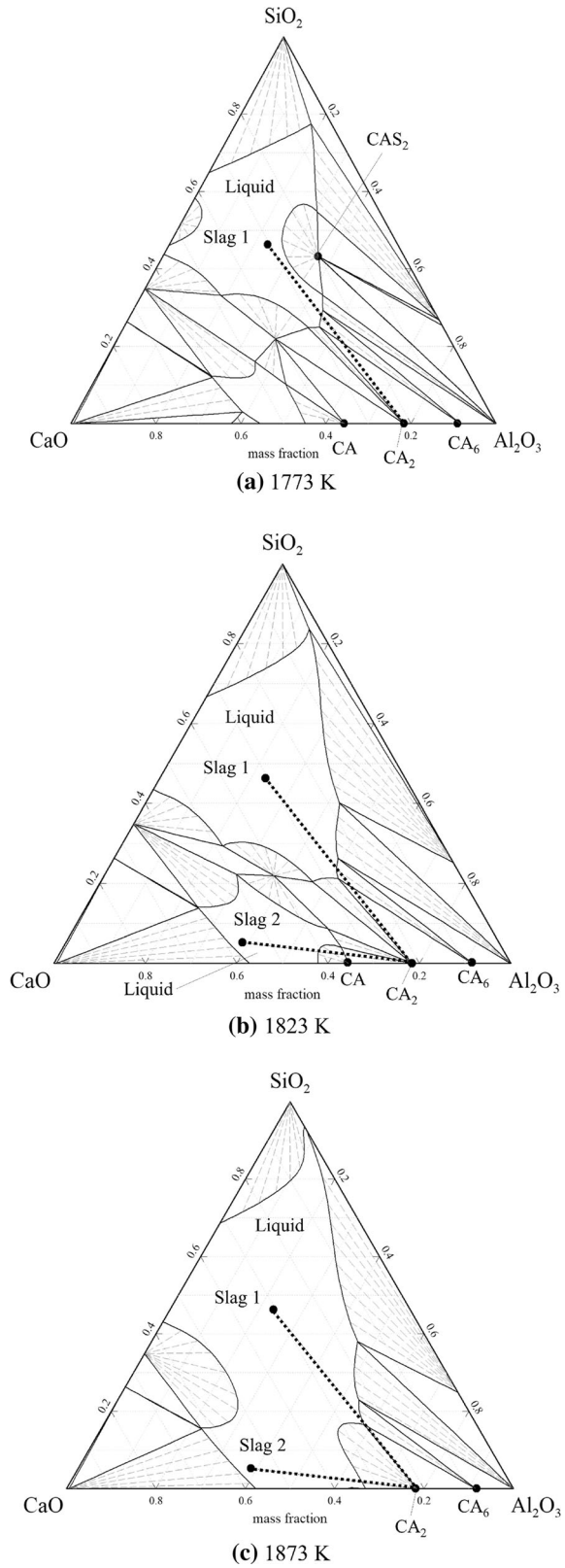

Fig. 5—Prediction of phase stability of the slag–CA_2 inclusion system using Factsage™ at (*a*) 1773 K (1500 °C) (*b*) 1823 K (1550 °C) (*c*) 1873 K (1600 °C).

Furthermore, the product layer might dissolve within the defined quenching time. Another important finding is that no concentration gradient of Ca was detected. This result supports the idea that the diffusion of CaO is much faster than the diffusion of Al_2O_3 in the system studied.

In the case of dissolution of CA_2 particle in slag 2 at 1823 K (1550 °C), formation of CA is thermodynamically favored. It is known that CA can be partially liquid,[38,39] therefore the product layer is most likely not dense enough to influence the dissolution process. At 1873 K (1600 °C), slag 2 reaches local equilibrium with CA_2, and there will be no reaction products.

In this study, the thermodynamic driving force for the particle dissolution is the Al_2O_3 concentration difference between slag–particle interface and the slag bulk. The reason of selecting Al_2O_3 as rate limiting species will be explained later in the text. The compositions of slag at the slag–particle interface for all experimental conditions were calculated using Factsage™ version 7.0 and summarized in Table I. The Al_2O_3 concentration difference is higher in slag 1 than in slag 2 at the same temperature, and it increases with increasing temperature. The density of slag was calculated based on the molar volume of constituents.[40] The viscosity of the slags, as calculated by Urbain's model,[40] decreases as temperature increases, with the viscosity of slag 1 being about an order of magnitude higher than that of slag 2.

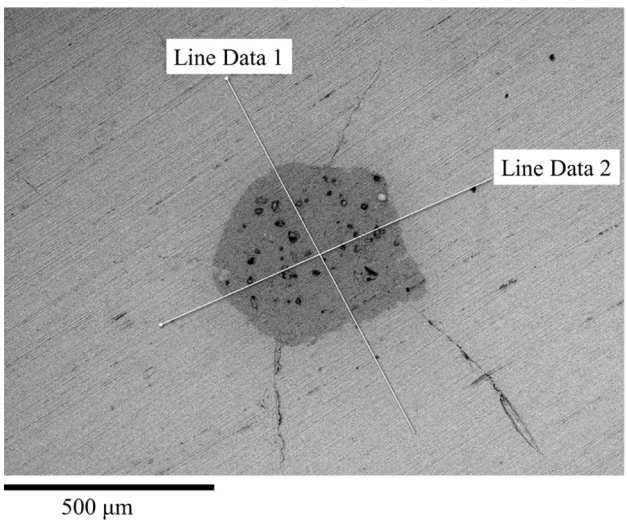

Fig. 6—Back scattered image of a CA_2 particle quenched after dissolving for 60 s at 1823 K (1550 °C) in slag 1.

B. *Dissolution Mechanism*

To understand the dissolution process, it is important to establish the rate controlling mechanism of the dissolution reaction. The shrinking core model (SCM) and the diffusion into a stagnant fluid model have both been applied to determine the dissolution mechanism of inclusions in steelmaking slags.[10,11,41,42] These models are used in this study and their development and applications can be found elsewhere.[10,41,43,44] This study assumes that the chemical reactions are not a rate limiting step because the high temperature of steelmaking reactions favors high reaction rates. Thus, reaction kinetics are likely controlled by the transport of elements to/from the interface. Based on these models, two different rate controlling steps are considered: (1) diffusion through a solid product layer, (2) mass transfer in slag with diffusion through a boundary layer.

In the present study, AlO_x^{y-} from the dissolved CA_2 particle is assumed to be the rate controlling species, as opposed to Ca^{2+}. The authors adapted a similar approach to that suggested by previous researchers[15] by focusing on the dissolution kinetics of spinel inclusions. The Ca^{2+} cation is smaller than the AlO_x^{y-} anions, and Ca^{2+} is expected to have higher diffusion coefficient than the AlO_x^{y-} anions. It has also been reported that the diffusion coefficients of AlO_x^{y-} and Ca^{2+} in a slag containing 40 CaO-20 Al_2O_3-40 wt pct SiO_2 at 1823 K (1550 °C) were 3.44×10^{-11} and

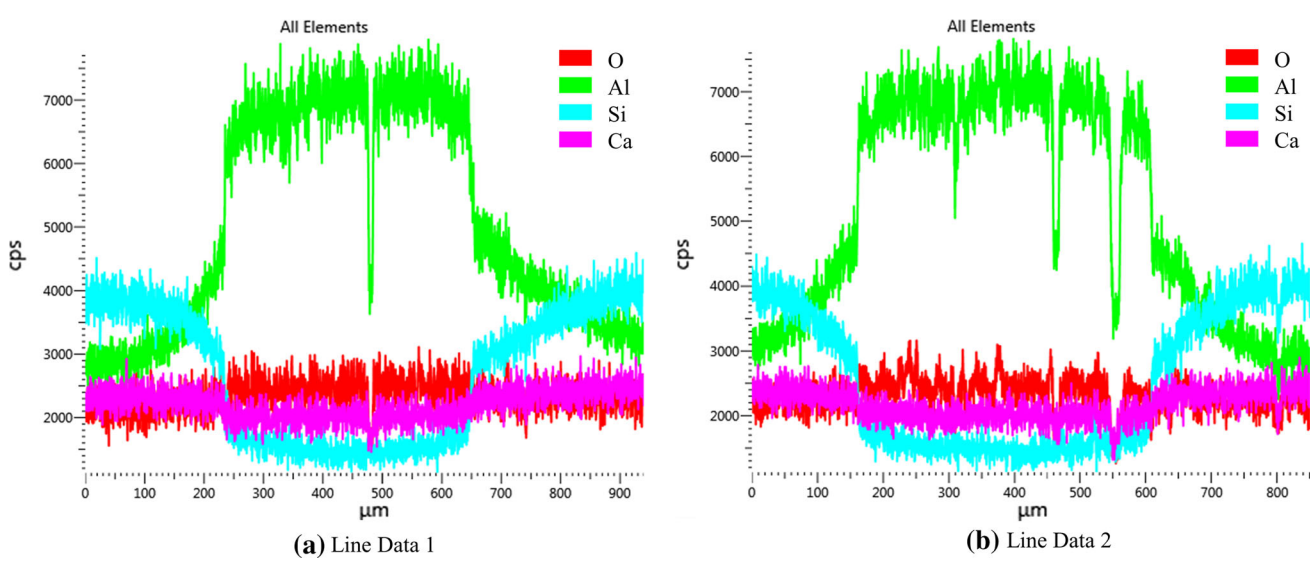

Fig. 7—EDS results of (*a*) Line Data 1 and (*b*) Line Data 2 analysis of the CA_2 particle shown in Fig. 8 (Color figure online).

Table I. Bulk Slag Composition, Experimental Temperatures, Saturation Compositions, Calculated Slag Viscosities, and the Concentration Differences of Al_2O_3

Slag	Composition (Wt Pct)	Temperature (K)	Slag Viscosity (Pa s)	Saturation Composition (Wt Pct)	Al_2O_3 Concentration Difference (mol/m^3)
1	$46.3SiO_2$-30.5CaO-$23.2Al_2O_3$	1773	9.5	$28.0SiO_2$-27.0CaO-$45.0Al_2O_3$	6098
		1823	6.5	$23.9SiO_2$-26.2CaO-$49.9Al_2O_3$	7407
		1873	4.3	$17.9SiO_2$-24.9CaO-$57.2Al_2O_3$	9339
2	$5.3SiO_2$-56.1CaO-$38.6Al_2O_3$	1823	0.49	$2.9SiO_2$-40.6CaO-$56.5Al_2O_3$	4713
		1873	0.37	$2.5SiO_2$-33.0CaO-$64.5Al_2O_3$	6817

5.11×10^{-10} m^2/s,[40] respectively. Therefore, AlO_x^{y-} diffusion becomes rate controlling. For simplicity, AlO_x^{y-} and Ca^{2+} are referred as Al_2O_3 and CaO, respectively, in the following text.

In the case of (1), product layer diffusion control, the SCM considers formation of a continuous dense product layer around the dissolving particle. Once the product layer is fully developed, dissolution is slower through solid reaction product than through liquid slag. Therefore, diffusion through the product layer becomes rate controlling to the entire dissolution process. Such a rate controlling mechanism results in a characteristic S shape curve. The mathematical expression of this controlling mechanism is provided in Eq. [4] and the total dissolution time τ is estimated using Eq. [5]. It is important to note that this approach provides a clear analytical solution of total dissolution time.

$$\frac{t}{\tau} = 1 - 3\left(\frac{R}{R_0}\right)^2 + 2\left(\frac{R}{R_0}\right)^3, \quad [4]$$

$$\tau = \frac{\rho R_0}{6D\Delta C}. \quad [5]$$

In the case of (2) diffusion through a boundary layer, it is assumed that a constant concentration gradient of the rate limiting species is built at the slag–particle interface once dissolution has started. The rate of particle radius change increases with the decrease of a particle's surface area-to-volume ratio. Using SCM, the mathematical expressions of this rate controlling step and total dissolution time are written as Eqs. [6] and [7]:

$$\frac{t}{\tau} = 1 - \left(\frac{R}{R_0}\right)^2, \quad [6]$$

$$\tau = \frac{\rho R_0^2}{2bD\Delta C}, \quad [7]$$

where ρ is molar density of the particle and is equal to 20,838 mol Al_2O_3/m^3. R is the equivalent radius at time t and R_0 is the initial equivalent radius at time zero. The constant b is a stoichiometric constant of CA_2 that reacts with slag and equals 1. D and ΔC denote the diffusion coefficient and the molar concentration difference of the rate limiting species, respectively. In Eq. [5], ΔC is the concentration difference of Al_2O_3 in the reaction product, whereas in Eq. [5] ΔC is the concentration difference of Al_2O_3 between the slag–particle interface and the slag bulk, shown in Table I.[10,15,42,45] Yan *et al.*[46] suggested a methodology to incorporate the effect of convection in the dissolution model for the boundary layer diffusion control. While their modeling results agreed well with previous experimental data, this methodology is not used in the current study because the particles were observed to move slowly and seldom rotated in the slag.

The diffusion into a stagnant fluid control model was based on the Fick's first and second laws of diffusion.[10,47] The mathematical expression of this model with moving boundary is shown in Eq. [8].[10] Parameter f is the fitting parameter that controls the shape of dissolution curve and it is strongly related to the slag viscosity. Dimensionless concentration, k is defined in Eq. [9]. C_i, C_0, and C_p are concentration of the rate limiting species at the inclusion–slag interface, in the slag bulk and in the inclusion, respectively. Feichtinger *et al.*[48] claimed that f varies from 0 to 1. $f = 0$ for slags with infinitely low viscosity, whereas $f = 1$ for slags with infinitely high viscosity. The diffusion into a stagnant fluid control model can be solved numerically as suggested by Lee *et al.*[10,48] In the present study, Eq. [8] was solved using the classical Runge–Kutta method.

$$\frac{dR}{dt} = \frac{kD}{R} - fk\sqrt{\frac{D}{\pi t}}, \quad [8]$$

$$k = \frac{C_i - C_0}{C_p - C_i}. \quad [9]$$

The dissolution mechanism can be determined by comparing the experimental results with the theoretical dissolution curves for each proposed dissolution mechanism. Figure 8 plots experimental normalized equivalent radii *vs* the normalized time for CA_2 particles that dissolved in slag 1 at 1773 K (1500 °C), where the solid triangles and squares represent data from two different experiments. The dashed, dotted, and dashed-dotted lines represent the predictions by the reaction product diffusion control SCM, boundary layer diffusion control SCM, and the diffusion into a stagnant fluid control model, respectively. The experimental data correspond closely to the SCM reaction product control. To confirm this mechanism, the authors studied the slag–particle interfaces by scanning electron microscope (SEM) as

shown in Figures 6 and 7. As stated before, no reaction product was found. Therefore, one can argue that this model can be applicable to predict the dissolution rate of CA_2 particles.

The experimental data also agree with predictions using the diffusion into a stagnant fluid control model. This model states that the concentration profile cannot be eliminated and the concentration profile evolves in an extended boundary layer. This is in good agreement with the detected boundary layer and concentration profiles as shown in Figures 6 and 7. It should be noted that the calculated value of f is 2.05. This is a higher value than those suggested by Feichtinger *et al.*[48] This is most likely due to the fact that viscosity of slag 1 at 1773 K is relatively higher than those studied by previous researchers.[10,48,49] One can argue that the direct application of this model is questionable for dissolution of particles in viscous fluids (> 9 Pa s). Further the range of values for f should be re-evaluated. Therefore, the dissolution mechanism remains unclear at the current stage of the study and further investigations will be carried out to characterize the particle–slag interface at various dissolution times in the future. We can conclude that the dissolution rate is slow due to high viscosity of the slag 1 at 1773 K and slag is likely to act like a solid product layer.

The dissolution profiles of the CA_2 particles dissolving in slag 1 at 1823 K and 1873 K (1550 °C and 1600 °C) are shown in Figures 9 and 10, respectively. In both cases, the majority of the experimental data agree with the predictions of the diffusion into a stagnant fluid control model. The applied f factors are 0.39 and 0.25. These values are low and reflects parabolic shape. It should be noted that there is a slight difference between the predictions of the stagnant fluid diffusion control model and the boundary layer diffusion control SCM. The boundary layer diffusion control SCM tends to underestimate the observed dissolution rate during the intermediate stage of the dissolution process (> 0.4 and < 0.85). Towards the end of the dissolution process, as both models converge to the normalized equivalent radius of 1, the difference between the two models further decreases.

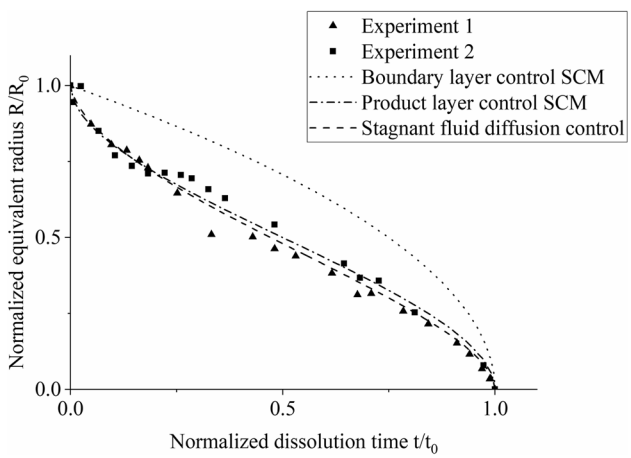

Fig. 8—Normalized dissolution profiles of CA_2 particles in molten slag 1 at 1773 K (1500 °C).

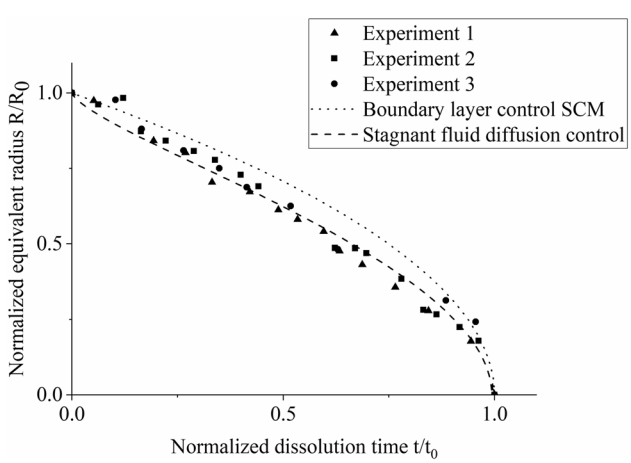

Fig. 9—Normalized dissolution profiles of CA_2 particles in molten slag 1 at 1823 K (1550 °C).

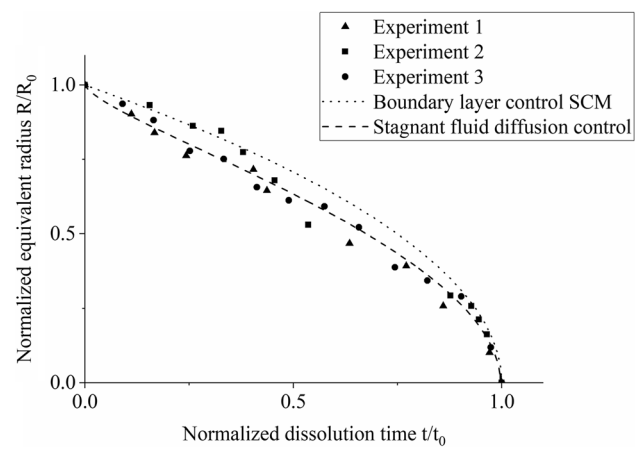

Fig. 10—Normalized dissolution profiles of CA_2 particles in molten slag 1 at 1873 K (1600 °C).

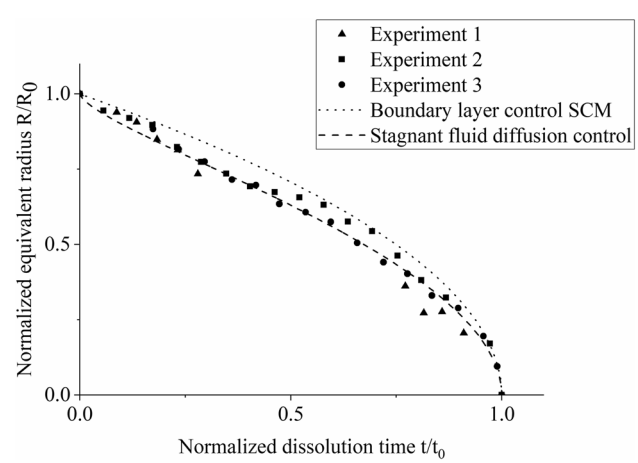

Fig. 11—Normalized dissolution profiles of CA_2 particles in molten slag 2 at 1823 K (1550 °C).

A comparison between the models' predictions and experimental data for the dissolution rate of CA_2 particles in slag 2 at 1823 K and 1873 K (1550 °C and 1600 °C) is shown in Figures 11 and 12, respectively. The diffusion into a stagnant fluid control model and boundary layer diffusion control SCM both predict well compared to the diffusion through reaction product control model. It can be suggested that the dissolution of the CA_2 particle at 1823 K and 1873 K (1550 °C and 1600 °C) is controlled by mass transport in the slag. Both modeling approaches can be used to determine the dissolution mechanism of a CA_2 particle in CaO-Al_2O_3-SiO_2 slags.

C. *Effect of Temperature on Dissolution Time*

The effect of temperature on the dissolution of CA_2 particles was studied by comparing the total dissolution time of inclusions in the slag 1 at three different temperatures: 1773 K, 1823 K, and 1873 K (1500 °C, 1550 °C, and 1600 °C). A comparison of the dissolution times is shown in Figure 13. The measured values for the equivalent radius of inclusions at time zero (R_0) were 135, 115, and 111 μm at temperatures 1773 K, 1823 K, and 1873 K (1500 °C, 1550 °C, and 1600 °C), respectively.

It is clear that the dissolution time decreases by increasing the temperature from 1773 K to 1823 K (1500 °C to 1550 °C) and then to 1873 K (1600 °C). This finding agrees with previous studies.[5,10,11,13] It is established that the important kinetics parameters, such as the diffusion coefficients, dissolution driving force, and reaction constants, will be enhanced when the temperature increases. The dissolution time was reduced from 393 to 238 to 120 seconds when temperature was increased from 1773 K to 1823 K and 1873 K (1500 °C to 1550 °C and 1600 °C). A similar trend is found for dissolution of CA_2 particles in slag 2 in the same temperature range.

D. *Effect of Slag Composition on Dissolution Time*

Figure 14 compares the dissolution times of CA_2 particles in slag 1 and slag 2 at 1773 K (1550 °C). The solid and hollow data points are from experiments with slag 1 and slag 2. The important difference between the two slags is the SiO_2 content. Slag 1 and slag 2 have 46.3 and 5 wt pct of SiO_2 content, respectively. The comparison includes all experiments of particles with a similar initial radius, in the range of 96–115 μm.

The dissolution time of CA_2 particles in slag 2 was approximately 70 seconds shorter than that for a similar sized particle in slag 1 at 1823 K (1550 °C). For both experiments in slag 1, the complete dissolution took more than 100 seconds while for experiments in slag 2, the dissolution time was approximately 50 seconds. Similar behavior was observed at 1873 K (1600 °C). A CA_2 particle of the same initial diameter took about 100 seconds longer to completely dissolve in high SiO_2 slag 1 than in low SiO_2 slag 2. As seen, the dissolution rate of a CA_2 particle is strongly influenced by the slag composition. Even though the thermodynamic driving force for dissolution is lower for slag 2 than slag 1, the

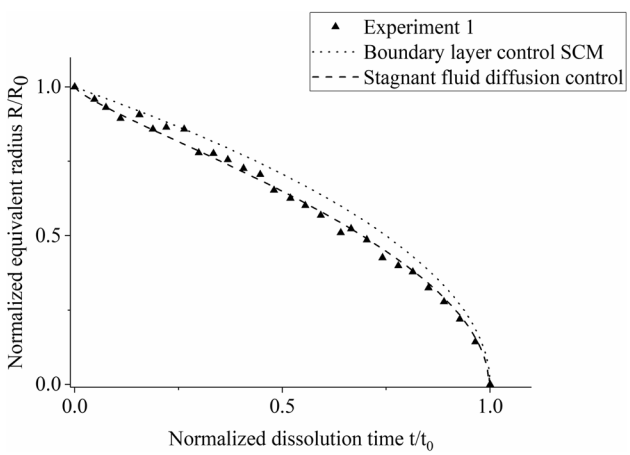

Fig. 12—Normalized dissolution profiles of CA_2 particles in molten slag 2 at 1873 K (1600 °C).

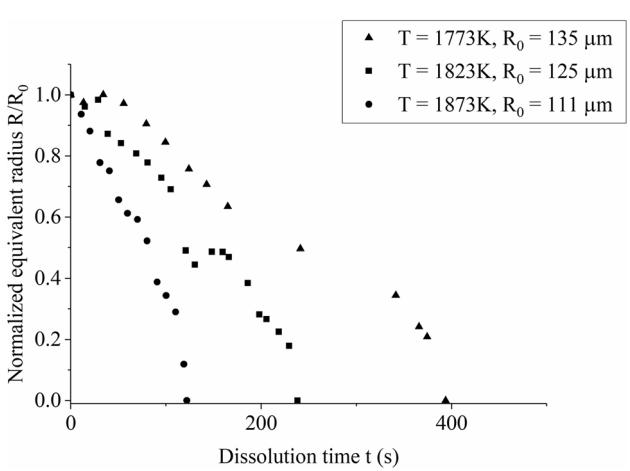

Fig. 13—Normalized equivalent radius *vs* total dissolution time of CA_2 particles in slag 1 at different temperatures.

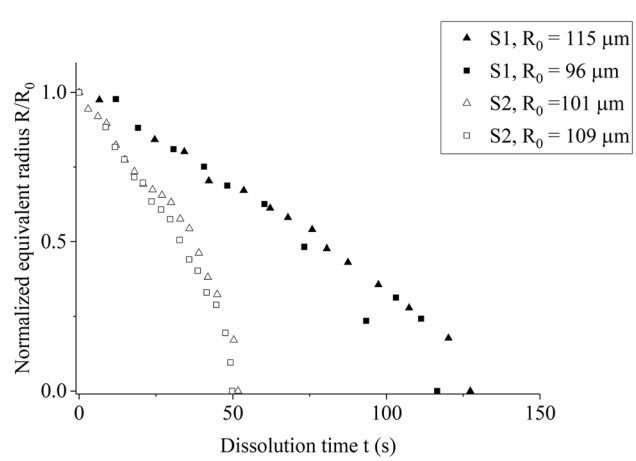

Fig. 14—Normalized equivalent radius *vs* total dissolution time of CA_2 particles in slag 1 (S1) and slag 2 (S2) at 1823 K (1550 °C).

Table II. Summary of Calculated Diffusion Coefficients *D* Using Different Models

Experimental Conditions (Slag-Temperature)	Product Layer (m^2/s)	Boundary Layer (m^2/s)	Stagnant Fluid (m^2/s)
S1-1773	2.11E−11	6.32E−11	5.64E−12
S1-1823		1.16E−10	2.62E−11
S1-1873		1.58E−10	2.75E−11
S2-1823		4.04E−10	7.34E−11
S2-1873		5.80E−10	6.35E−11

dissolution time of the CA_2 particles is shorter in slag 2. This is most likely related to the high diffusion coefficients of Al_2O_3 in slag 2.

E. *Prediction of Diffusion Coefficient*

The diffusion coefficient of Al_2O_3 in the slag was calculated using both modeling approaches in this study. Equations [6] and [8] were applied for each experimental condition and the diffusion coefficients are summarized in Table II. According to the Eyring relation,[48] the diffusion coefficient is inversely proportional to the viscosity. Since the viscosity of slag 1 is higher than that of slag 2, the diffusion coefficient of Al_2O_3 is expected to be higher in slag 2 than in slag 1. On inspection of Table II, the calculated diffusion coefficients are in good agreement with the Eyring relation[48] and support a mass transfer controlled process. This finding is valid using both modeling results.

The diffusion coefficient of Al_2O_3 at 1773 K (1500 °C) is 5.64×10^{-12} m^2/s using the diffusion into stagnant fluid model. This is the lowest value compared to other calculated values using diffusion through a solid product layer model and diffusion through a boundary layer model (2.1×10^{-11} and 6.32×10^{-11}, respectively). It should be noted that this value is similar to the diffusion coefficient of Al_2O_3 in CA_2 used in a study on inclusion modification. Tabatabaei *et al.*[50] developed a mathematical model to predict the modification of Al_2O_3 during Ca treatment in the ladle. In their work, they extrapolated Eq. [10][51] to predict the diffusion coefficient of Al_2O_3 in CA_2 at 1873 K. This equation was originally proposed by Ali *et al.*[51] based on experimental data of Al_2O_3 diffusion in CA_2 at 1623 K, 1673 K, and 1723 K. Using Eq. [10], the diffusion coefficient of Al_2O_3 would be 1.6×10^{-12} m^2/s at 1773 K (1500 °C). This indicates that the calculated values for diffusion coefficient in liquid slag 1 are as low as values for diffusion coefficient in solid at 1773 K (1500 °C).

$$D = 49.562 \times 10^{-10}\, e^{-\frac{28,400}{RT}}. \qquad [10]$$

The diffusion coefficients of Al_2O_3 at 1823 K are in the same range as previously reported values. Monaghan *et al.*[31] studied the dissolution of alumina inclusions in slag which represents a similar composition as slag 1 in this study at 1823 K. They applied the boundary layer model based on SCM and the reported Al_2O_3 diffusion coefficient was 1.60×10^{-10} and 1.87×10^{-10} m^2/s. In this study, the calculated value is 1.16×10^{-10} m^2/s using the same modeling approach. Liu *et al.*[10] investigated the dissolution of Al_2O_3 particles in a CaO-Al_2O_3-SiO_2 slag from 1743 K to 1903 K (1470 °C to 1630 °C). They applied the diffusion into stagnant fluid model and the reported diffusion coefficients of Al_2O_3 were 3.3×10^{-11}, 3.4×10^{-11}, and 3.8×10^{-11} m^2/s at 1823 K (1550 °C). Appling the same model in this study, the obtained diffusion coefficient was 2.62×10^{-11} m^2/s. It can be concluded that there is an agreement between reported and calculated values for diffusion coefficient of Al_2O_3 when same dissolution model was applied. Therefore, the slight difference between the suggested values by two models is related to the difference in modeling approaches. As discussed before, the purpose of this study is not to suggest a specific dissolution model for inclusion dissolution studies. The authors plan to discuss their own modeling approach in a subsequent paper in the future.

IV. COMMENTS ON LIMITATIONS OF CSLM TECHNIQUE FOR INCLUSION DISSOLUTION

The CSLM has proven to be a useful tool in studying phenomena related to steelmaking processes such as '*in-situ*' real-time observation and measurement of inclusion dissolution and agglomeration, phase transformations, and solidification. All these directly affect the productivity of the steelmaking process. Based on the authors' current experience observing inclusion dissolution, the slag needs to be low in transition elements such as iron, manganese, chromium, or titanium which affect the transparency of the system and hinder *in situ* observation of the process.[45,52] In our preliminary experiments, use of slag containing 0.9 wt pct Fe_2O_3 did not much affect the transparency of slag. Moreover, Soll-Morris and co-workers[53] performed similar CSLM experiments and they were able to observe the dissolution of Al_2O_3 in SiO_2-CaO-Al_2O_3-FeO_x slag with a maximum 9.16 wt pct FeO_x. where the liquid slag was not transparent but the inclusion boundary can be identified.

The size of the particle which can be observed in the CSLM is in the range of 50 to 1000 μm. The smaller (< 30 μm) inclusions of interest to steelmakers dissolve too quickly for study. In addition, (i) The relative density of particle should be considered since floating or suspended particles are required in order to make accurate observations; (ii) The heating rate should be carefully set to ensure that inclusion dissolution starts at

the intended temperature, as slow heating rates will likely be dissolved prematurely. High heating rates can lead to temperature overshoot; (iii) The particle should have relatively low porosity to inhibit bubble formation during inclusion dissolution or it might be difficult to identify the particle–slag phase boundary; (iv) For accurate measurements of inclusion dissolution, the amount of particle dissolved in slag should not much affect the driving force, and the mass of the particle should be less than 0.1 wt pct of the slag.[42]

V. CONCLUSIONS

The dissolution behavior of CA_2 particles in the CaO-SiO_2-Al_2O_3 slags was studied *in situ* in the temperature range of 1773 K to 1873 K (1500 °C to 1600 °C) by using CSLM. This study offers novel data on dissolution of CA_2 inclusions in the steelmaking slags, which has not been reported in open literature. The following conclusions can be drawn from the present study:

1. The dissolution time for CA_2 particles of approximately 100 μm in size was between 50 and 120 seconds for the slag compositions used at 1823 K (1550 °C). The dissolution rate of CA_2 particles increases with an increase in temperature in both slags.
2. Slag composition has a significant effect on the dissolution rate. The dissolution time is reduced significantly in low SiO_2 slag (slag 2). The faster dissolution rates in slag 2 can be related to the higher diffusion coefficients and the lower viscosity values than those in slag 1 at any temperature. These findings were in good agreement with the Eyring relation[48] and support a mass transfer controlled process.
3. The dissolution of CA_2 is controlled by mass transfer in the investigated slag systems at 1823 K and 1873 K (1550 °C and 1600 °C). The dissolution mechanism at 1773 K (1500 °C) remains unclear at the current stage of the study and further investigations will be carried out to characterize the particle–slag interface at various dissolution times in the future. We can conclude that the dissolution rate is slow due to high viscosity of the slag 1 at 1773 K and slag is likely to act like a solid product layer.
4. The diffusion coefficients were in reasonable agreement with those reported in the literature. The calculated diffusion coefficients for the systems studied ranged between 5.64×10^{-12} and 5.8×10^{-10} m^2/s. At 1773 K (1500 °C), the value for diffusion coefficient in slag 1 was 5.64×10^{-12} m^2/s. The high viscosity slag slows down diffusion to an extent that is similar to diffusion through a solid product layer.

ACKNOWLEDGMENTS

The authors would like to thank the Natural Sciences and Engineering Research Council of Canada (NSERC) and Canada Foundation for Innovation John Evans Leaders Fund (CFI JELF, Project Number: 32826) for funding this research.

REFERENCES

1. K. Kawakami, T. Taniguchi, and K. Nakashima: *Tetsu-to-Hagane*, 2007, vol. 93, pp. 743–52.
2. S. Yang, L. Zhang, L. Sun, J. Li, and K.D. Peaslee: *Iron Steel Technol.*, 2012, vol. 9, pp. 245–58.
3. S.K. Choudhary and A. Ghosh: *ISIJ Int.*, 2008, vol. 48, pp. 1552–59.
4. S. Sridhar and A.W. Cramb: *Metall. Mater. Trans. B*, 2000, vol. 31B, pp. 406–10.
5. M. Valdez, K. Prapakorn, A.W. Cramb, and S. Sridhar: *Ironmak. Steelmak.*, 2002, vol. 29, pp. 47–52.
6. B.G. Thomas and L. Zhang: *Rev. Lit. Arts Am.*, 2001, vol. 41, pp. 1181–93.
7. L. Jonsson and P. Jönsson: *ISIJ Int.*, 1996, vol. 36, pp. 1127–34.
8. M. Hallberg, P.G. Jönsson, T.L.I. Jonsson, and R. Eriksson: *Scand. J. Metall.*, 2005, vol. 34, pp. 41–56.
9. Y. Miki, H. Kitaoka, T. Sakuraya, and T. Fujii: *ISIJ Int.*, 1992, vol. 32, pp. 142–49.
10. J. Liu, F. Verhaeghe, M. Guo, B. Blanpain, and P. Wollants: *J. Am. Ceram. Soc.*, 2007, vol. 90, pp. 3818–24.
11. K.W. Yi, C. Tse, J.H. Park, M. Valdez, A.W. Cramb, and S. Sridhar: *Scand. J. Metall.*, 2003, vol. 32, pp. 177–84.
12. M. Valdez, K. Prapakorn, A.W. Cramb, and S. Seetharaman: *Steel Res.*, 2001, vol. 72, pp. 291–97.
13. B.J. Monaghan, S.A. Nightingale, L. Chen, and G.A. Brooks: in *International Conference on Molten Slags Fluxes and Salts*, 2004, pp. 585–94.
14. B.J. Monaghan, L. Chen, and J. Sorbe: *Ironmak. Steelmak.*, 2005, vol. 32, pp. 258–64.
15. B.J. Monaghan and L. Chen: *Ironmak. Steelmak.*, 2006, vol. 33, pp. 323–30.
16. X. Yu, R.J. Pomfret, and K.S. Coley: *Metall. Mater. Trans. B*, 1997, vol. 28B, pp. 275–79.
17. K.H. Sandhage and G.J. Yurek: *J. Am. Ceram. Soc.*, 1991, vol. 74, pp. 1941–54.
18. S. Taira, K. Nakashima, and K. Mori: *ISIJ Int.*, 1993, vol. 33, pp. 116–23.
19. K.H. Sandhage and G.J. Yurek: *J. Am. Ceram. Soc.*, 1988, vol. 71, pp. 478–89.
20. K.H. Sandhage and G.J. Yurek: *J. Am. Ceram. Soc.*, 1990, vol. 73, pp. 3633–42.
21. K.H. Sandhage and G.J. Yurek: *J. Am. Ceram. Soc.*, 1990, vol. 73, pp. 3643–49.
22. H. Chikama, H. Shibata, T. Emi, and M. Suzuki: *Mater. Trans.*, 1996, vol. 37, pp. 620–26.
23. H. Shibata, Y. Arai, M. Suzuki, and T. Emi: *Metall. Mater. Trans. B*, 2000, vol. 31B, pp. 981–91.
24. H. Shibata, H. Yin, S. Yoshinaga, T. Emi, and M. Suzuki: *ISIJ Int.*, 1998, vol. 38, pp. 149–56.
25. B. Coletti, B. Blanpain, S. Vantilt, and S. Sridhar: *Metall. Mater. Trans. B*, 2003, vol. 34B, pp. 533–38.
26. Y. Kang, B. Sahebkar, P.R. Scheller, K. Morita, and D. Sichen: *Metall. Mater. Trans. B*, 2011, vol. 42B, pp. 522–34.
27. P. Misra, V. Chevrier, S. Sridhar, and A.W. Cramb: *Metall. Mater. Trans. B*, 2000, vol. 31B, pp. 1135–39.
28. C. Orrling, S. Sridhar, and A.W. Cramb: *ISIJ Int.*, 2000, vol. 40, pp. 877–85.
29. W. Mu, N. Dogan, and K.S. Coley: *Metall. Mater. Trans. B*, 2017, vol. 48B, pp. 2092–2103.
30. W. Mu, N. Dogan, and K.S. Coley: *Metall. Mater. Trans. B*, 2017, vol. 48B, pp. 2379–88.
31. B.J. Monaghan and L. Chen: *J. Non. Cryst. Solids*, 2004, vol. 347, pp. 254–61.
32. M. Lind and L. Holappa: *Metall. Mater. Trans. B*, 2010, vol. 41B, pp. 359–66.
33. M.W. Chapman: University of Wollongong, 2009.
34. S. Jonas, F. Nadachowski, and D. Szwagierczak: *Ceram. Int.*, 1998, vol. 24, pp. 211–16.

35. S. Jonas, F. Nadachowski, and D. Szwagierczak: *Ceram. Int.*, 1999, vol. 25, pp. 77–84.
36. W.D. Callister: *Materials Science and Engineering an Introduction*, 2007.
37. G. Fiquet, P. Richet, and G. Montagnac: *Phys. Chem. Miner.*, 1999, vol. 27, pp. 103–11.
38. D. Yang, X. Wang, G. Yang, P. Wei, and J. He: *Steel Res. Int.*, 2014, vol. 85, pp. 1517–24.
39. N. Verma, P.C. Pistorius, R.J. Fruehan, M.S. Potter, H.G. Oltmann, and E.B. Pretorius: *Metall. Mater. Trans. B*, 2012, vol. 43B, pp. 830–40.
40. *Slag Atlas*, 3rd ed., V.D. Eisenhuttenleute, ed., *Slag Atlas*, 2nd ed., Verlag Stahleisen GmbH, Dusseldorf, 1995.
41. O. Levenspiel: *Chemical Reaction Engineering*, 3rd ed., Wiley, New York, 1998, pp. 566–88.
42. S.H. Lee, C. Tse, K.W. Yi, P. Misra, V. Chevrier, C. Orrling, S. Sridhar, and A.W. Cramb: *J. Non Cryst. Solids*, 2001, vol. 282, pp. 41–48.
43. F.J. Vermolen, C. Vuik, E. Javierre, and S. Van Der Zwaag: *Nonlinear Anal. Model Control*, 2005, vol. 10, pp. 257–92.
44. J.Y. Choi, H.G. Lee, and J.S. Kim: *ISIJ Int.*, 2002, vol. 42, pp. 852–60.
45. J. Liu, M. Guo, P.T. Jones, F. Verhaeghe, B. Blanpain, and P. Wollants: *J. Eur. Ceram. Soc.*, 2007, vol. 27, pp. 1961–72.
46. P. Yan, B.A. Webler, P.C. Pistorius, and R.J. Fruehan: *Metall. Mater. Trans. B*, 2015, vol. 46B, pp. 2414–18.
47. R.J. Aguerre, J.F. Gabitto, and J. Chirife: *Int. J. Food Sci. Technol.*, 1985, vol. 20, pp. 623–29.
48. S. Feichtinger, S.K. Michelic, Y.B. Kang, and C. Bernhard: *J. Am. Ceram. Soc.*, 2014, vol. 97, pp. 316–25.
49. S. Michelic, J. Goriupp, S. Feichtinger, Y.B. Kang, C. Bernhard, and J. Schenk: *Steel Res. Int.*, 2015, vol. 86, pp. 1–11.
50. Y. Tabatabaei, K.S. Coley, G.A. Irons, and S. Sun: *Metall. Mater. Trans. B*, 2018, vol. 49B, pp. 375–87.
51. M.M. Ali, S.J. Raina, and V.K. Singh: *Cem. Concr. Res.*, 1989, vol. 19, pp. 47–52.
52. B.J. Monaghan, S.A Nightingale, L. Chen, and G. A. Brooks: *Mater. Sci.*, 2004, pp. 585–94.
53. H. Soll-Morris, C. Sawyer, Z.T. Zhang, G.N. Shannon, J. Nakano, and S. Sridhar: *Fuel*, 2009, vol. 88, pp. 670–82.